PARAMETRIC CHARACTERIZATION AND ESTIMATION OF BI-AZIMUTH AND DELAY DISPERSION OF INDIVIDUAL PATH COMPONENTS

Xuefeng Yin [1)], **Troels Pedersen** [1)], **Nicolai Czink** [3), 2)] **and Bernard H. Fleury** [1), 2)]

[1)] *Information and Signals Division, Department of Communication Technology, Aalborg University, Aalborg, Denmark*
[2)] *Forschungszentrum Telekommunikation Wien (ftw.), Vienna, Austria*
[3)] *Institut für Nachrichtentechnik und Hochfrequenztechnik, Technische Universität Wien, Vienna, Austria*

ABSTRACT

In this contribution, we derive a distribution that is suitable for characterizing biazimuth (azimuth of arrival and azimuth of departure) and delay dispersion of individual path components in the response of the radio channel. This distribution maximizes the entropy under the constraint that its first and second moments are specified. We propose to use the density function of the derived distribution to characterize the shape of the biazimuth-delay power spectrum of individual path components. The applicability of this characterization in real conditions is assessed using measurement data.

Key words: Path component, von-Mises-Fisher distribution, biazimuth-delay dispersion, power spectrum, density function.

1. INTRODUCTION

Due to the heterogeneity of the propagation environment, the response of the radio channel is the superposition of a certain number of components. Each component, which we call a "path component", is contributed by an electromagnetic wave propagating along a path from the transmitter (Tx) to the receiver (Rx). Along this path, the wave interacts with a certain number of objects called scatterers. Due to the geometrical and electromagnetic properties of the scatterers, a propagation path may be dispersive in delay, direction of departure, direction of arrival, polarizations, as well as in Doppler frequency when the environment is time-variant. As a consequence, an individual path component may be spread or dispersed in these dispersion dimensions.

Recently, estimation of dispersive characteristics of individual path components has gained much attention. Conventional methods rely on estimation of the channel response and any characterizing functions derived from this response. An example of a characterizing function is the power spectrum. A traditional estimate of the power spectrum is the Bartlett spectrum, i.e. the spectrum calculated using the Bartlett beamformer [1]. However, due to the ambiguity function of the measurement equipment, the path components in the Bartlett spectrum are blurred and consequently, their spreads are artificially increased. In recent years, several methods based on parametric models have been proposed to estimate the nominal azimuth and azimuth spread of path components at one side of the link [2], [3], [4]. These estimators make use of the assumption that the azimuth power spectrum of individual path components exhibits a shape close to the density function of a distribution, like the uniform distribution within a certain interval [3], the (truncated) Gaussian distribution [2], [3] and the von-Mises distribution [4].

Recently, the density function of a bivariate von-Mises-Fisher distribution has been proposed to characterize the shape of the biazimuth (azimuth of departure (AoD) and azimuth of arrival (AoA)) power spectrum of individual path components [5]. The von-Mises-Fisher distribution maximizes the entropy under the constraint that its first and second moments are specified. In [5], the proposed characterization method is assessed in real conditions using measurement data.

In this contribution, we derive an entropy-maximizing distribution suitable for characterizing biazimuth-delay dispersion of individual path components. More specifically, the density function of this distribution is used to characterize the shape of the biazimuth-delay power spectrum of individual path components. The density function is parameterized by some free parameters. To identify these parameters, we postulate that in the case where a path component is slightly dispersed, the proposed density function is close to a truncated multivariate Gaussian density function. Experimental investigations assess the applicability of the proposed characterization in real situations.

The organization of this contribution is as follows. In Section 2, we derive the entropy-maximizing biazimuth-delay density function. In Section 3, the signal model is

This work was jointly supported by the Network of Excellence in Wireless COMmunications (NEWCOM), Elektrobit Testing Oy and the Austrian Kplus Program.

presented. Section 4 shows the results and discussions of the experimental investigations. Finally concluding remarks are stated in Section 5.

2. ENTROPY-MAXIMIZING BIAZIMUTH-DELAY DENSITY FUNCTION

Following the nomenclature in [6], we use a unit vector $\mathbf{\Omega}$ to characterize a direction. This vector has its initial point anchored at the origin O of a coordinate system specified in the region surrounding the array of interest, and terminal point located on a unit sphere $\mathbb{S}_2$ centered at O. In the case of horizontal-only propagation, the terminal point of $\mathbf{\Omega}$ is located on a unit circle $\mathbb{S}_1$. The one-to-one relation between $\mathbf{\Omega}$ and the azimuth ϕ is in this case

$$\mathbf{\Omega} = \boldsymbol{e}(\phi) \doteq [\cos(\phi), \sin(\phi)]^{\mathrm{T}} \tag{1}$$

with $[\cdot]^{\mathrm{T}}$ denoting transposition.

Among all distributions on $\mathbb{S}_1$, the von-Mises distribution maximizes the entropy provided the first moment

$$\boldsymbol{\mu}_{\mathbf{\Omega}} \doteq \int \mathbf{\Omega} f(\mathbf{\Omega}) \mathrm{d}\mathbf{\Omega}$$

is specified [6], [7]. Here, $f(\mathbf{\Omega})$ denotes the density function of any distribution on $\mathbb{S}_1$. Notice that $\int f(\mathbf{\Omega})\mathrm{d}\mathbf{\Omega} = 1$. The density function of the von-Mises distribution is given by [8, P. 36]

$$f(\mathbf{\Omega}) = \frac{1}{2\pi I_0(\kappa)} \exp\{\kappa \bar{\mathbf{\Omega}}^{\mathrm{T}} \mathbf{\Omega}\} \tag{2}$$

with $I_0(\cdot)$ denoting the modified Bessel function of the first kind and order 0, $\kappa \geq 0$ being the concentration parameter, and $\bar{\mathbf{\Omega}} \in \mathbb{S}_1$. For $\kappa > 0$, $\bar{\mathbf{\Omega}}$ is the mode of $f(\mathbf{\Omega})$ and $\bar{\mathbf{\Omega}} = \|\boldsymbol{\mu}_{\mathbf{\Omega}}\|^{-1} \boldsymbol{\mu}_{\mathbf{\Omega}}$ holds. Here, $\|\cdot\|$ denotes the Euclidean norm. It is shown in [6] that the root second central moment of a distribution on $\mathbb{S}_1$, i.e. the direction spread $\sigma_{\mathbf{\Omega}}$, is uniquely determined by the norm of the first moment: $\sigma_{\mathbf{\Omega}} = \sqrt{1 - \|\boldsymbol{\mu}_{\mathbf{\Omega}}\|^2}$. It follows from this result that the von-Mises distribution also maximizes the entropy under the constraint that the mode, provided that it exists, and the direction spread are specified. In [9], the von-Mises density function has been used to characterize the shape of the azimuth power spectrum of individual path components.

Among all distributions on $\mathbb{S}_1 \times \mathbb{S}_1$, the generalized von-Mises-Fisher distribution [7] maximizes the entropy under the constraints that the first moments

$$\boldsymbol{\mu}_{\mathbf{\Omega}_i} \doteq \int \mathbf{\Omega}_i f(\mathbf{\Omega}_1, \mathbf{\Omega}_2) \mathrm{d}\mathbf{\Omega}_1 \mathrm{d}\mathbf{\Omega}_2, \quad i = 1, 2 \tag{3}$$

and second moments in the matrix

$$\mathbf{\Sigma}_{\mathbf{\Omega}_1 \mathbf{\Omega}_2} \doteq \int \mathbf{\Omega}_1 \mathbf{\Omega}_2^{\mathrm{T}} f(\mathbf{\Omega}_1, \mathbf{\Omega}_2) \mathrm{d}\mathbf{\Omega}_1 \mathrm{d}\mathbf{\Omega}_2 \tag{4}$$

are specified. In (3) and (4), $f(\mathbf{\Omega}_1, \mathbf{\Omega}_2)$ is the density function of any distribution on $\mathbb{S}_1 \times \mathbb{S}_1$. The density function of the generalized von-Mises-Fisher distribution is of the form [7]

$$f(\mathbf{\Omega}_1, \mathbf{\Omega}_2) = C \cdot \exp\{\boldsymbol{a}_1^{\mathrm{T}} \mathbf{\Omega}_1 + \boldsymbol{a}_2^{\mathrm{T}} \mathbf{\Omega}_2 + \mathbf{\Omega}_1^{\mathrm{T}} \boldsymbol{A} \mathbf{\Omega}_2\}, \tag{5}$$

where C denotes a normalization constant, while $\boldsymbol{a}_1$, $\boldsymbol{a}_2 \in \mathbb{R}^{2\times 1}$ and $\boldsymbol{A} \in \mathbb{R}^{2\times 2}$ are free parameters. This density function has been proposed in [5] to characterize the shape of the biazimuth power spectrum of individual path components. In this case, $\mathbf{\Omega}_1, \mathbf{\Omega}_2$ are written to be $\mathbf{\Omega}_i = \boldsymbol{e}(\phi_i)$, $i = 1, 2$ with ϕ_1 and ϕ_2 denoting the AoD and AoA respectively. The expressions of the free parameters $\boldsymbol{a}_1$, $\boldsymbol{a}_2$ and $\boldsymbol{A}$ are identified in [5]. Experimental investigations reported in this reference showed that this density function can be used to characterize the shape of the biazimuth power spectrum of individual path components.

Following the same approach as used in [5], we derive in the sequel a distribution suitable to describe dispersion of individual path components in $\mathbf{\Omega}_1$, $\mathbf{\Omega}_2$ and propagation delay τ. More specifically, the density function of the sought distribution characterizes the shape of the biazimuth-delay power spectrum of individual path components.

We define the parameter vector $\boldsymbol{\psi} \doteq [\mathbf{\Omega}_1^{\mathrm{T}}, \mathbf{\Omega}_2^{\mathrm{T}}, \tau]^{\mathrm{T}}$. The density function $f(\boldsymbol{\psi})$ of the distribution maximizing the entropy with its first moment

$$\boldsymbol{\mu}_{\boldsymbol{\psi}} \doteq \int \boldsymbol{\psi} f(\boldsymbol{\psi}) \mathrm{d}\boldsymbol{\psi}$$

and second moments in the matrix

$$\mathbf{\Sigma}_{\boldsymbol{\psi}} \doteq \int \boldsymbol{\psi}\boldsymbol{\psi}^{\mathrm{T}} f(\boldsymbol{\psi}) \mathrm{d}\boldsymbol{\psi}$$

specified, is of the form [7]

$$f(\boldsymbol{\psi}) \propto \exp\{\boldsymbol{b}^{\mathrm{T}} \boldsymbol{\psi} + \boldsymbol{\psi}^{\mathrm{T}} \boldsymbol{B} \boldsymbol{\psi}\}, \tag{6}$$

where $\boldsymbol{b} \in \mathbb{R}^{5\times 1}$ and $\boldsymbol{B} \in \mathbb{R}^{5\times 5}$ are free parameters.

The biazimuth-delay distribution induced by the above entropy-maximizing distribution via the mapping $[\phi_1, \phi_2, \tau] \mapsto [\boldsymbol{e}(\phi_1)^{\mathrm{T}}, \boldsymbol{e}(\phi_2)^{\mathrm{T}}, \tau]$ has density function

$$f(\phi_1, \phi_2, \tau) = f(\boldsymbol{\psi})|_{\boldsymbol{\psi} = [\boldsymbol{e}(\phi_1)^{\mathrm{T}}, \boldsymbol{e}(\phi_2)^{\mathrm{T}}, \tau]^{\mathrm{T}}}. \tag{7}$$

To identify the expressions of the vector $\boldsymbol{b}$ and the matrix $\boldsymbol{B}$, we assume that in the case where dispersion of individual path components is small, the density function in (7) is close to a truncated multivariate Gaussian density function. Define the parameter vector $\boldsymbol{\omega} \doteq [\phi_1, \phi_2, \tau]^{\mathrm{T}}$. The truncated Gaussian density function is of the form

$$f_{\mathrm{G}}(\boldsymbol{\omega}) \propto \frac{1}{\det(\mathbf{\Sigma}_{\boldsymbol{\omega}})^{1/2}} \exp\{-\frac{1}{2}(\boldsymbol{\omega} - \boldsymbol{\mu}_{\boldsymbol{\omega}})^{\mathrm{T}} \mathbf{\Sigma}_{\boldsymbol{\omega}}^{-1}(\boldsymbol{\omega} - \boldsymbol{\mu}_{\boldsymbol{\omega}})\}, \tag{8}$$

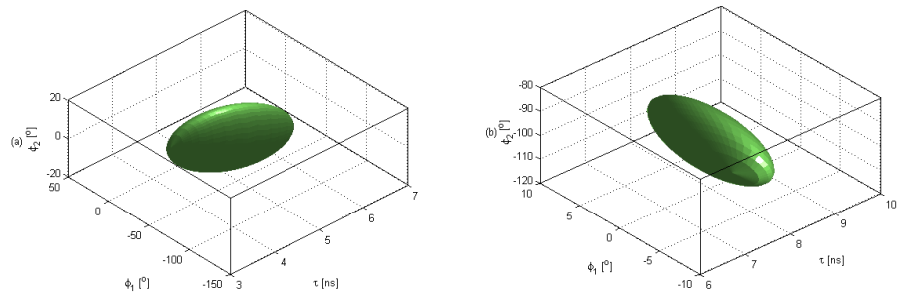

	$\bar{\tau}$ [ns]	$\bar{\phi}_1$ [°]	$\bar{\phi}_2$ [°]	σ_τ [ns]	κ_1	σ_{ϕ_1} [°]	κ_2	σ_{ϕ_2} [°]	ρ_{12}	ρ_1	ρ_2
(a)	5	−40	0	1	5	25.6	10	18.1	−0.4	−0.3	−0.3
(b)	8	0	−100	0.5	50	8.1	30	10.5	−0.5	0.6	−0.2

Figure 1. 3*dB-spread surfaces calculated using the density function (13) with parameter settings given above.*

with $\boldsymbol{\mu}_{\boldsymbol{\omega}} \doteq [\bar{\phi}_1, \bar{\phi}_2, \bar{\tau}]^{\mathrm{T}}$ denoting the mode of $f_{\mathrm{G}}(\boldsymbol{\omega})$ and

$$\boldsymbol{\Sigma}_{\boldsymbol{\omega}} \doteq \begin{bmatrix} \sigma_{\phi_1}^2 & \rho_{\phi_1\phi_2}\sigma_{\phi_1}\sigma_{\phi_2} & \rho_{\phi_1\tau}\sigma_{\phi_1}\sigma_\tau \\ \rho_{\phi_1\phi_2}\sigma_{\phi_1}\sigma_{\phi_2} & \sigma_{\phi_2}^2 & \rho_{\phi_2\tau}\sigma_{\phi_2}\sigma_\tau \\ \rho_{\phi_1\tau}\sigma_{\phi_1}\sigma_\tau & \rho_{\phi_2\tau}\sigma_{\phi_2}\sigma_\tau & \sigma_\tau^2 \end{bmatrix}. \quad (9)$$

Notice that strictly speaking, the traditional meaning of σ_{ϕ_1}, σ_{ϕ_2}, $\rho_{\phi_1\phi_2}$, $\rho_{\phi_1\tau}$ and $\rho_{\phi_2\tau}$ as second-order central moments of a 3-variate Gaussian distribution does not apply anymore to (8), due to the fact that the azimuth ranges are bounded. However, these parameters provide good approximations of these moments when σ_{ϕ_1}, σ_{ϕ_2} are small. For notational convenience, we use ρ_1, ρ_2 and ρ_{12} to denote $\rho_{\phi_1\tau}$, $\rho_{\phi_2\tau}$ and $\rho_{\phi_1\phi_2}$ respectively.

In the case where dispersion of a path component is sufficiently small, the following approximations hold:

$$\begin{aligned} (\phi_1 - \bar{\phi}_1)(\phi_2 - \bar{\phi}_2) &\approx \\ &[\boldsymbol{e}(\phi_1) - \boldsymbol{e}(\bar{\phi}_1)]^{\mathrm{T}} \boldsymbol{R} [\boldsymbol{e}(\phi_2) - \boldsymbol{e}(\bar{\phi}_2)] \quad (10) \\ (\phi_i - \bar{\phi}_i)(\tau - \bar{\tau}) &\approx \\ &[\boldsymbol{e}(\phi_i) - \boldsymbol{e}(\bar{\phi}_i)]^{\mathrm{T}} \boldsymbol{e}(\bar{\phi}_i + \pi/2)(\tau - \bar{\tau}) \quad (11) \\ (\phi_i - \bar{\phi}_i)^2 &\approx \|\boldsymbol{e}(\phi_i) - \boldsymbol{e}(\bar{\phi}_i)\|^2 \quad (12) \end{aligned}$$

with $i \in \{1, 2\}$ and

$$\boldsymbol{R} \doteq \begin{bmatrix} \cos(\bar{\phi}_1 - \bar{\phi}_2) & -\sin(\bar{\phi}_1 - \bar{\phi}_2) \\ \sin(\bar{\phi}_1 - \bar{\phi}_2) & \cos(\bar{\phi}_1 - \bar{\phi}_2) \end{bmatrix}.$$

The motivation for selecting the matrix $\boldsymbol{R}$ and the meaning of this matrix are described in [5]. Notice that subtraction of azimuth variables arising in the right-hand side in (8) and the left-hand sides in (10)–(12) is defined in such a way that the resulting angle lies in the range $[-\pi, \pi)$.

Inserting (10), (11) and (12) into (8) and identifying (7) and (8), yields for (7)

$$\begin{aligned} f(\phi_1, \phi_2, \tau) \;=\; & D \cdot \exp\{\alpha_1 \cos(\phi_1 - \bar{\phi}_1) + \alpha_2 \cos(\phi_2 - \bar{\phi}_2) \\ & + (\tau - \bar{\tau})[\alpha_3 \sin(\phi_1 - \bar{\phi}_1) + \alpha_4 \sin(\phi_2 - \bar{\phi}_2)] \\ & + \alpha_5 (\tau - \bar{\tau})^2 + \alpha_6 \cos[(\phi_1 - \bar{\phi}_1) - (\phi_2 - \bar{\phi}_2)]\}, \quad (13) \end{aligned}$$

where D is a normalization factor, while $\alpha_1, \ldots, \alpha_6$ are given by

$$\begin{aligned} \alpha_1 &= \frac{1}{a}\big[\kappa_1(\rho_2^2 - 1) + \sqrt{\kappa_1\kappa_2}(\rho_{12} - \rho_1\rho_2)\big], \\ \alpha_2 &= \frac{1}{a}\big[\kappa_2(\rho_1^2 - 1) + \sqrt{\kappa_1\kappa_2}(\rho_{12} - \rho_1\rho_2)\big], \\ \alpha_3 &= \sqrt{\kappa_1}(\rho_{12}\rho_2 - \rho_1)/(a\sigma_\tau), \\ \alpha_4 &= \sqrt{\kappa_2}(\rho_{12}\rho_1 - \rho_2)/(a\sigma_\tau), \\ \alpha_5 &= \frac{1}{2a}\frac{1 - \rho_{12}^2}{\sigma_\tau^2},\ \alpha_6 = \frac{\sqrt{\kappa_1\kappa_2}(\rho_1\rho_2 - \rho_{12})}{a} \end{aligned}$$

with $\kappa_i = 1/\sigma_{\phi_i}^2$, $i = 1, 2$ denoting the concentration parameters in AoD and AoA respectively and $a = \rho_2^2 + \rho_{12}^2 + \rho_1^2 - 2\rho_{12}\rho_1\rho_2 - 1$.

Fig. 1 depicts the 3dB-spread surface

$$\left\{(\phi_1, \phi_2, \tau) : f(\phi_1, \phi_2, \tau) = \frac{1}{2} f(\bar{\phi}_1, \bar{\phi}_2, \bar{\tau})\right\} \quad (14)$$

computed using the density function (13) for the two parameter settings also reported in this figure. We observe that these surfaces are close to ellipsoids when κ_1 and κ_2 are large. This is reasonable as the density function (13) is close to the density function of a truncated multivariate Gaussian distribution (8) in the case of small dispersion. Notice that the 3dB-spread surface of the multivariate Gaussian distribution is an ellipsoid.

3. SIGNAL MODEL

We consider the case where the path components are dispersed in biazimuth and delay. Following the nomenclature in [6], the continuous-time (complex baseband representation of the) output signal of the Rx array reads

$$\begin{aligned} \boldsymbol{Y}(t) \;=\; & \int_{-\pi}^{+\pi}\int_{-\pi}^{+\pi}\int_{-\infty}^{+\infty} \boldsymbol{c}_2(\phi_2)\boldsymbol{c}_1(\phi_1)^{\mathrm{T}} \boldsymbol{s}(t - \tau) \\ & h(t; \phi_1, \phi_2, \tau)\mathrm{d}\phi_1\mathrm{d}\phi_2\mathrm{d}\tau + \boldsymbol{W}(t). \quad (15) \end{aligned}$$

In (15), $\boldsymbol{Y}(t) \in \mathbb{C}^{M_2 \times 1}$ contains the output signals of the Rx array elements observed at time instance t, $\boldsymbol{s}(t) \in \mathbb{C}^{M_1 \times 1}$ denotes the complex baseband representation of the transmitted signal, and the function $h(t; \phi_1, \phi_2, \tau)$ is referred to as the (time-variant) biazimuth-delay spread function of the propagation channel. In a scenario where the electromagnetic energy propagates from the Tx to the Rx via D paths, $h(t; \phi_1, \phi_2, \tau)$ can be decomposed as

$$h(t; \phi_1, \phi_2, \tau) = \sum_{d=1}^{D} h_d(t; \phi_1, \phi_2, \tau). \tag{16}$$

The summand $h_d(t; \phi_1, \phi_2, \tau)$ denotes the dth path component. The noise vector $\boldsymbol{W}(t) \in \mathbb{C}^{M_2 \times 1}$ in (15) is a circularly symmetric, spatially and temporally white complex Gaussian process with component spectral height σ_w^2. Finally, $\boldsymbol{c}_i(\phi) \doteq [c_{i,1}(\phi), \ldots, c_{i,m_i}(\phi), \ldots, c_{i,M_i}(\phi)]^{\mathrm{T}} \in \mathbb{C}^{M_i \times 1}$, $i = 1, 2$ are the responses of the Tx array and the Rx array respectively.

We assume that the biazimuth-delay spread functions $h_d(t; \phi_1, \phi_2, \tau)$, $d \in \{1, \ldots, D\}$ are uncorrelated complex (zero-mean) orthogonal stochastic measures, i.e.

$$\begin{aligned} \mathrm{E}[h_d(t; \phi_1, \phi_2, \tau)^* h_{d'}(t'; \phi_1', \phi_2', \tau')] = P_d(\phi_1, \phi_2, \tau) \\ \delta_{dd'} \delta_{tt'} \delta(\phi_1 - \phi_1') \delta(\phi_2 - \phi_2') \delta(\tau - \tau'), \end{aligned} \tag{17}$$

where $(\cdot)^*$ denotes complex conjugate, $\delta_{..}$ and $\delta(\cdot)$ represent the Kronecker delta and Dirac delta function respectively, t and t' are discrete time instants at which the spread function are sampled, and

$$P_d(\phi_1, \phi_2, \tau) \doteq \mathrm{E}[|h_d(t; \phi_1, \phi_2, \tau)|^2]$$

is the biazimuth-delay power spectrum of the dth path component. Identity (17) implies that the spread functions of different individual path components or at different observation instants are uncorrelated. With the above assumptions, $h(t; \phi_1, \phi_2, \tau)$ is also an uncorrelated complex zero-mean stochastic measure specified by

$$\begin{aligned} \mathrm{E}[h(t; \phi_1, \phi_2, \tau)^* h(t'; \phi_1', \phi_2', \tau')] = P(\phi_1, \phi_2, \tau) \\ \delta_{tt'} \delta(\phi_1 - \phi_1') \delta(\phi_2 - \phi_2') \delta(\tau - \tau') \end{aligned} \tag{18}$$

with $P(\phi_1, \phi_2, \tau) = \sum_{d=1}^{D} P_d(\phi_1, \phi_2, \tau)$.

The biazimuth-delay spectrum $P_d(\phi_1, \phi_2, \tau)$ describes the manner the average power of the dth path component is distributed with respect to AoD, AoA and delay. We assume that

$$P_d(\phi_1, \phi_2, \tau) = P_d \cdot f(\phi_1, \phi_2, \tau; \boldsymbol{\theta}_d),$$

where P_d represents the total average power of the dth path component and $f(\phi_1, \phi_2, \tau; \boldsymbol{\theta}_d)$ is the density function (13) with path-specific parameters

$$\boldsymbol{\theta}_d \doteq [\bar{\phi}_{1,d}, \bar{\phi}_{2,d}, \bar{\tau}_d, \kappa_{1,d}, \kappa_{2,d}, \sigma_{\tau_d}, \rho_{1,d}, \rho_{2,d}, \rho_{12,d}].$$

Clearly, the center of gravity of $P_d(\phi_1, \phi_2, \tau)$ coincides with $(\bar{\phi}_{1,d}, \bar{\phi}_{2,d}, \bar{\tau}_d)$, i.e. the location at which the density function $f(\phi_1, \phi_2, \tau; \boldsymbol{\theta}_d)$ exhibits its maximum. The shape of $P_d(\phi_1, \phi_2, \tau)$ is determined jointly by $\kappa_{1,d}, \kappa_{2,d}, \sigma_{\tau_d}, \rho_{1,d}, \rho_{2,d}$ and $\rho_{12,d}$.

Table 1. Setting of the measurement equipment.

Carrier frequency	5.25 GHz
Bandwidth	200 MHz
Chip frequency	100 MHz
Code length	255 Chips
Tx array height	1.53 m
Rx array height	0.82 m

Let $\boldsymbol{\theta}$ denote a vector containing the model parameters in (15)

$$\boldsymbol{\theta} \doteq [\sigma_w^2, P_1, P_2, \ldots, P_D, \boldsymbol{\theta}_1, \boldsymbol{\theta}_2, \ldots, \boldsymbol{\theta}_D].$$

A stochastic maximum likelihood estimator of $\boldsymbol{\theta}$ can be easily derived [10] for the case where the spread functions of the path components are Gaussian. Due to the property expressed in (17), the spread functions of distinct path components or at different time instants are independent. The SAGE algorithm [11] can be easily implemented as a low-complexity approximation of the maximum likelihood estimator. Due to the space limitation, the descriptions of the maximum likelihood estimator and the SAGE algorithm are omitted in this paper.

4. EXPERIMENTAL INVESTIGATIONS

The measurement data were collected using the MIMO wideband radio channel sounder Elektrobit Propsound CS [12] [13]. The setting of the equipment is reported in Table 1. The Tx and Rx were both equipped with two identical 50-element dual-polarized omni-directional arrays (See Fig. 2). The polarization direction of the elements is $\pm 45^\circ$ slanted with respect to the vertical.

The measurement experiment was conducted in a big hall. During the measurement procedure, the hall was crowded with people moving around. These movements introduced time variations of the channel response. The positions of the Rx and Tx were kept fixed during the measurement procedure. Fig. 3 (a) and Fig. 3 (b) show a photograph of the surroundings of the Tx and the Rx respectively. Fig. 4 depicts the map of the premises. We notice that the Rx position is in the hall and the Tx is located at the entrance of a corridor. The data of 900 measurement cycles were collected within a period of 60 s. A measurement cycle refers to the interval within which all 50×50 subchannels are sounded once.

In order to maintain low computational complexity, the measurement data collected using two identical subarrays of the Tx and Rx arrays are considered. Each subarray consists of 9 dual-polarized elements uniformly spaced on a cylinder (See Fig. 2). Fig. 5 depicts the estimated

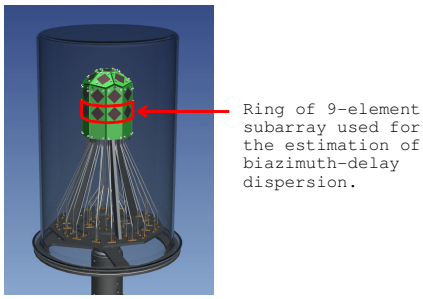

Figure 2. Illustration of the antenna arrays used in the Tx and the Rx of the channel sounder.

(a) Surroundings of the Tx.

(b) Surroundings of the Rx.

Figure 3. Photographs of the premises where the measurement experiment was conducted.

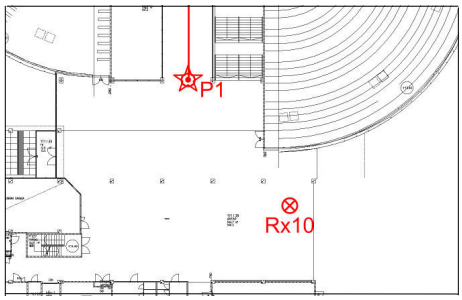

Figure 4. Map of the premises where the measurement experiment was conducted. The Tx and Rx locations are marked with "P1" and "Rx10" respectively.

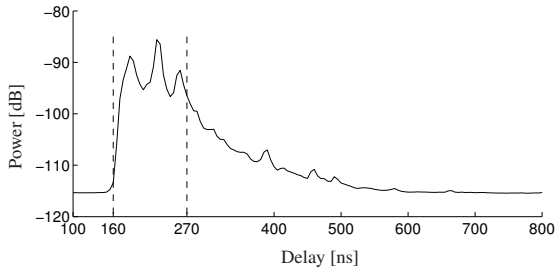

Figure 5. Estimated delay power spectrum.

delay power spectrum obtained by averaging the squared responses of the 81 subchannels of the 9×9 MIMO system. Again, to limit the computational effort the observation samples collected from delay 160 ns to delay 270 ns are considered in the estimation process.

In the SAGE algorithm, the dynamic range for the path power estimates is set to be 30 dB with respect to the maximum power estimate. The Bartlett beamformer [1] is used to initialize the path parameter estimates. The parameters that the Bartlett beamformer is incapable to estimate are set to certain predefined values. So, the estimates of the concentration parameters $\kappa_{1,d}$, $\kappa_{2,d}$, $d = 1, \ldots, D$ are set to 50 and the estimates of the coefficients $\rho_{1,d}, \rho_{2,d}, \rho_{12,d}$, $d = 1, \ldots, D$ equal 0. With this setting it is assumed a priori that the path components are close to being specular and that no dependency occurs across the considered dispersion dimensions.

After 10 SAGE iteration cycles, the parameter estimates of 20 path components are obtained. Table 2 reports the values of these estimates. The mean of the delay spread estimates of these components is 5.0 ns. The AoD spread estimates range from 4.4° to 16.2° with a mean equal to 9.0°. The AoA spread estimates range from 3.2° to 8.8° with a mean 5.0°. The difference between the AoA and AoD spread estimates can be attributed to the different structures of the environments surrounding the Tx and the Rx. From these results we observe that in a closed environment, e.g. in a corridor where the Tx is located, path components exhibit larger angular spreads than in an open environment, like the hall where the Rx is located.

Fig. 6 depicts $\text{Bartlett}(\hat{\boldsymbol{\Sigma}})$, $\text{Bartlett}(\boldsymbol{\Sigma}(\hat{\boldsymbol{\theta}}))$ and the estimated power spectrum $\hat{P}(\phi_1, \phi_2, \tau)$. The notations "$\text{Bartlett}(\hat{\boldsymbol{\Sigma}})$" and "$\text{Bartlett}(\boldsymbol{\Sigma}(\hat{\boldsymbol{\theta}}))$" denote the Bartlett spectrum calculated from respectively the sample covariance matrix and the covariance matrix computed based on the parameter estimate $\hat{\boldsymbol{\theta}}$. The estimated power spectrum $\hat{P}(\phi_1, \phi_2, \tau)$ is given by

$$\hat{P}(\phi_1, \phi_2, \tau) = \sum_{d=1}^{20} \hat{P}_d \cdot f(\phi_1, \phi_2, \tau; \hat{\boldsymbol{\theta}}_d), \qquad (19)$$

where $\hat{\boldsymbol{\theta}}_d$ denotes the estimate of the path-specific parameter $\boldsymbol{\theta}_d$. Note that although the biazimuth power spectra are plotted versus delay in Fig. 6, the power spectrum

of individual path components is estimated in AoA, AoD and delay jointly.

From Fig. 6 we observe that the estimated power spectra of individual path components are more concentrated than the corresponding footprints observed in $\mathrm{Bartlett}(\boldsymbol{\Sigma}(\hat{\boldsymbol{\theta}}))$. The blurring effect observed in $\mathrm{Bartlett}(\boldsymbol{\Sigma}(\hat{\boldsymbol{\theta}}))$ is due to the product of the ambiguity functions of the Tx and Rx array responses in azimuth. $\mathrm{Bartlett}(\hat{\boldsymbol{\Sigma}})$ and $\mathrm{Bartlett}(\boldsymbol{\Sigma}(\hat{\boldsymbol{\theta}}))$ are observed to be similar. In the following, the ratio $\mathrm{tr}[\boldsymbol{\Sigma}_{\mathrm{S}}(\hat{\boldsymbol{\theta}})]/\mathrm{tr}[\hat{\boldsymbol{\Sigma}}]$ is calculated, which can be conceived as the fraction of the signal power extracted from the sample covariance matrix. Here, $\mathrm{tr}[\cdot]$ denotes the trace of the matrix given as an argument. The signal-only covariance matrix $\boldsymbol{\Sigma}_{\mathrm{S}}(\hat{\boldsymbol{\theta}})$ is calculated using the parameter estimate $\hat{\boldsymbol{\theta}}$ with the noise variance estimate $\hat{\sigma}_w^2$ set to zero. This ratio equals $87.6\ \%$ for the considered case.

Although $\mathrm{Bartlett}(\hat{\boldsymbol{\Sigma}})$ and $\mathrm{Bartlett}(\boldsymbol{\Sigma}(\hat{\boldsymbol{\theta}}))$ in Fig. 6 are observed to be similar, their significant global and local maxima slightly differ. This difference might be due to the fact that in the parameter estimation process, the assumption of horizontal-only propagation is used. However, from the photographs shown in Fig. 3 we see that this assumption may not hold for all propagation paths. This inconsistency may introduce estimation errors as shown by further simulation studies. Another reason which might lead to this effect is that the derived density function (13) only provides an approximation to the shape of the effective power spectrum of individual path components. Estimation errors might result in the case where the difference is significant.

Fig. 7 depicts the estimated 3dB-spread surfaces (14) with the true path component parameters replaced by their estimates. The color of the surfaces codes the path power estimates according to the included color scale. We observe that some of the surfaces are not symmetric with respect to the axes of the delay, the AoD and the AoA. This effect indicates dependency of dispersion of individual path components across different dispersion dimensions. Some recent published works, e.g. [9], assume that dispersion of individual propagation paths in different dimensions (e.g. in delay and in AoA) is independent. Clearly, this assumption does not hold for some of the estimated path components in the investigated propagation environment. Further investigations are necessary in order to assess whether this observation is valid for all types of environments or not.

5. CONCLUSIONS

In this contribution, we derived a distribution which is suitable for characterizing biazimuth (azimuth of arrival and azimuth of departure) and delay dispersion of individual path components in the response of the propagation channel. This distribution maximizes the entropy under the constraint that its first and second moments are

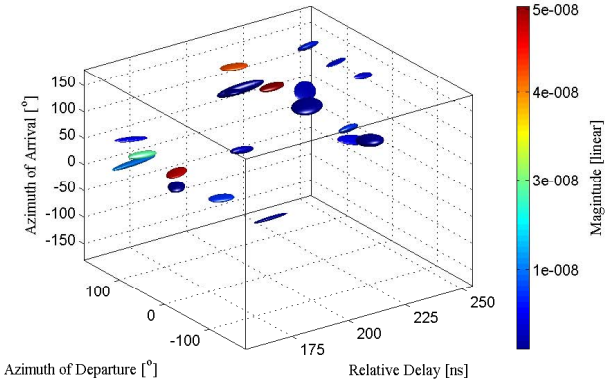

Figure 7. Estimated 3dB-spread surfaces of individual dispersed path components. The color of the surfaces codes the path power estimates according to the color scale reported on the right.

specified. The density function of the distribution characterizes the shape of the biazimuth-delay power spectrum of individual path components.

Preliminary experimental investigations were conducted to assess the applicability of the proposed characterization in real situations. From the obtained results we observed that dispersion of the path components in both azimuths and delay is much smaller than that one might infer from the corresponding footprints in the Bartlett spectrum. Moreover, the estimated power spectra of some path components are not symmetric with respect to the axes of the delay, the azimuth of arrival and the azimuth of departure. This indicates dependency across different dispersion dimensions. The results also show that the characterization method should include dispersion in elevation.

REFERENCES

1. M. Bartlett, "Smoothing periodograms from time series with continuous spectra," *Nature*, vol. 161, 1948.

2. T. Trump and B. Ottersten, "Estimation of nominal direction of arrival and angular spread using an array of sensors," *Signal Processing*, vol. 50, pp. 57–69, Apr. 1996.

3. O. Besson and P. Stoica, "Decoupled estimation of DoA and angular spread for spatially distributed sources," *IEEE Trans. Signal Processing*, vol. 49, pp. 1872–1882, 1999.

4. C. B. Ribeiro, E. Ollila, and V. Koivunen, "Stochastic maximum likelihood method for propagation parameter estimation," in *Proceedings of the 15th IEEE In-*

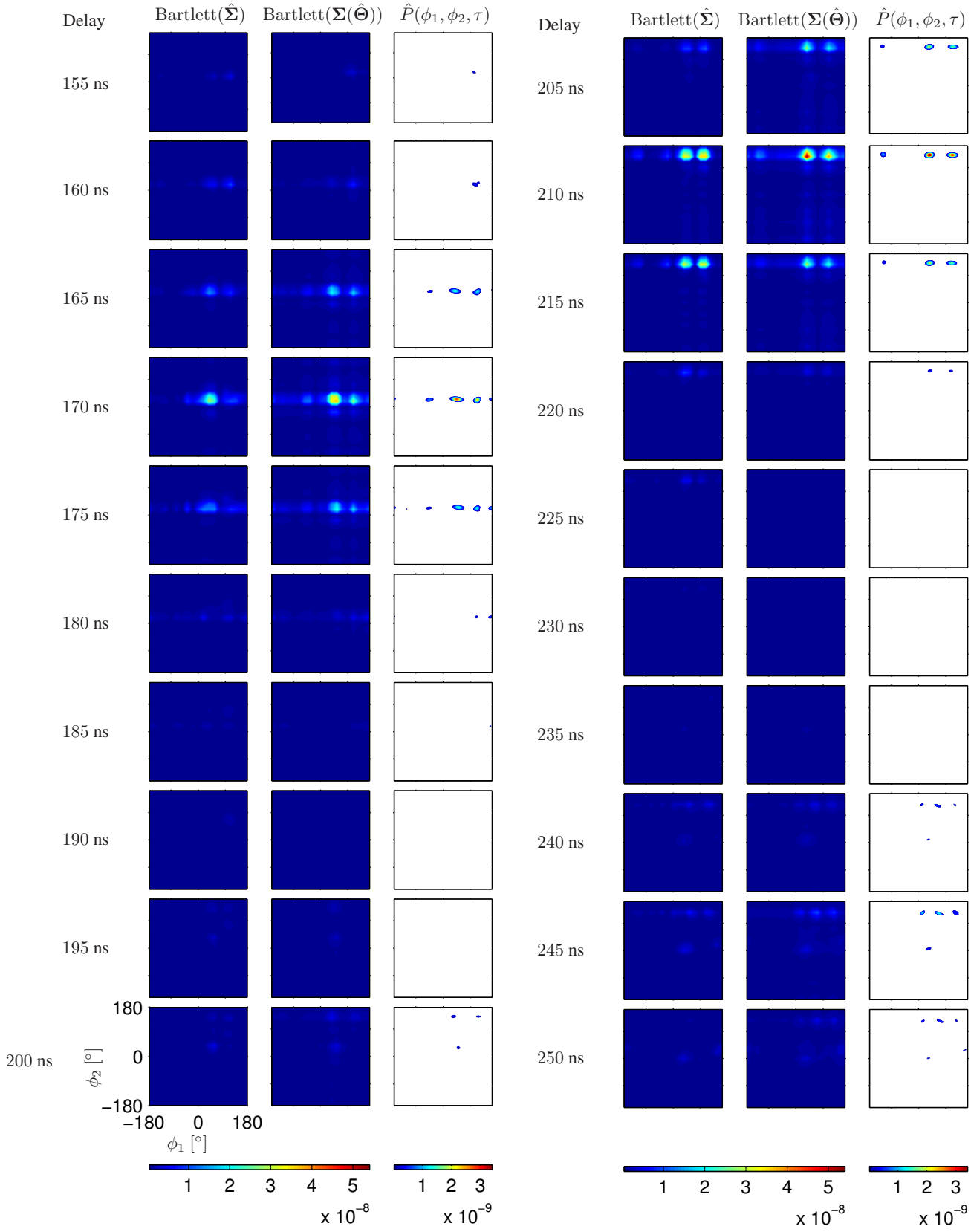

Figure 6. Estimated biazimuth-delay power spectrum.

Table 2. Estimates of the parameters of individual path components.

d	$\bar{\tau}_d$ ns	$\bar{\phi}_{1,d}$ [°]	$\bar{\phi}_{2,d}$ [°]	σ_{τ_d} ns	$\kappa_{1,d}$	$\sigma_{1,d}$ [°]	$\kappa_{2,d}$	$\sigma_{2,d}$ [°]	$\rho_{1,d}$	$\rho_{2,d}$	$\rho_{12,d}$	$P_d[10^{-7}]$	P_d [dB]
1	210	40	146	4.7	56.3	7.6	203.8	4.0	0.1	0.0	0.1	3.8	0
2	170	50	28	4.4	22.5	12.1	265.0	3.5	0.5	0.0	−0.3	3.5	−0
3	210	124	146	4.7	37.5	9.4	320.0	3.2	−0.3	0.0	−0.1	3.1	−1
4	170	126	26	4.9	95.0	5.9	176.3	4.3	−0.3	−0.2	0.4	1.8	−3
5	165	120	20	9.4	33.8	9.9	111.3	5.4	0.7	−0.4	−0.6	1.0	−6
6	170	−50	26	4.3	43.8	8.7	321.3	3.2	−0.3	−0.1	0.4	0.7	−7
7	210	−130	148	4.0	103.8	5.6	147.5	4.7	0.4	0.1	0.0	0.7	−7
8	245	136	138	4.2	57.5	7.6	90.0	6.0	0.3	0.0	−0.5	0.6	−8
9	245	74	136	4.2	36.3	9.5	290.0	3.4	0.4	0.2	−0.7	0.6	−8
10	175	176	26	5.9	116.3	5.3	210.0	4.0	−0.4	−0.8	0.5	0.5	−9
11	245	36	6	5.8	35.0	9.7	65.0	7.1	0.0	−0.8	0.4	0.5	−9
12	245	14	138	3.7	170.0	4.4	260.0	3.6	0.3	−0.3	0.7	0.3	−11
13	200	56	32	4.5	96.3	5.8	107.5	5.5	0.2	−0.4	−0.1	0.3	−11
14	250	168	30	4.8	16.3	14.2	52.5	7.9	0.5	0.2	0.9	0.3	−12
15	175	−134	22	6.4	71.3	6.8	163.8	4.5	0.2	−0.1	−0.8	0.2	−12
16	210	−38	146	5.7	12.5	16.2	73.8	6.7	0.2	0.0	0.3	0.2	−14
17	210	−178	148	4.2	13.8	15.5	66.3	7.0	−0.1	0.1	−0.1	0.1	−15
18	195	50	150	2.9	56.3	7.6	298.8	3.3	−0.1	−0.1	−0.2	0.1	−16
19	170	50	0	3.2	30.0	10.5	157.5	4.6	0.3	0.2	0.4	0.1	−16
20	210	110	110	7.9	52.5	7.9	42.5	8.8	−0.5	0.6	−0.3	0.05	−19
Mean				5.0	57.8	9.0	171.1	5.0	0.1	-0.10	0.0		

ternational Symposium on Personal, Indoor and Mobile Radio Communications (PIMRC), vol. 3, Sept. 5-8 2004.

5. X. Yin, T. Pedersen, N. Czink, and B. H. Fleury, "Parametric characterization and estimation of bi-azimuth dispersion of path components," in *Proceedings of the 7th IEEE International Workshop on Signal Processing Advances for Wireless Communications (SPAWC)*, Nice, France, July 2006.

6. B. H. Fleury, "First- and second-order characterization of direction dispersion and space selectivity in the radio channel," *IEEE Trans. Information Theory*, no. 6, pp. 2027–2044, Sept. 2000.

7. K. V. Mardia, "Statistics of directional data," *Journal of the Royal Statistical Society. Series B (Methodological)*, vol. 37, pp. 349–393, 1975.

8. K. V. Mardia and P. E. Jupp, *Directional Statistics*. John Wiley and Sons, Ltd., 2000.

9. C. B. Ribeiro, A. Richter, and V. Koivunen, "Stochastic maximum likelihood estimation of angle- and delay-domain propagation parameters," in *Proceedings of the 16th IEEE International Symposium on Personal, Indoor and Mobile Radio Communications (PIMRC)*, Berlin, Germany, 2005.

10. H. Krim and M. Viberg, "Two decades of array signal processing research: the parametric approach," *IEEE Trans. Signal Processing*, vol. 13, pp. 67–94, 1996.

11. B. H. Fleury, M. Tschudin, R. Heddergott, D. Dahlhaus, and K. L. Pedersen, "Channel parameter estimation in mobile radio environments using the SAGE algorithm," *IEEE Journal on Selected Areas in Communications*, vol. 17, no. 3, pp. 434–450, Mar. 1999.

12. N. Czink, E. Bonek, X. Yin, and B. H. Fleury, "Cluster angular spreads in a MIMO indoor propagation environment," in *Proceedings of the 16th IEEE International Symposium on Personal, Indoor and Mobile Radio Communications (PIMRC)*, Berlin, Germany, 2005.

13. E. Bonek, N. Czink, V. M. Holappa, M. Alatossava, L. Hentilä, J. Nuutinen, and A. Pal, "Indoor MIMO measurements at 2.55 and 5.25 GHz - a comparison of temporal and angular characteristics," in *Proceedings of the 15th IST Mobile Summit*, 2006.